Local manifestations of thickness-dependent topology and edge states in the topological magnet $MnBi_2Te_4$

Felix Lüpke,[1,2,*] Anh D. Pham,[1] Yi-Fan Zhao,[3] Ling-Jie Zhou,[3] Wenchang Lu,[4,5] Emil Briggs,[4] Jerzy Bernholc,[4,5] Marek Kolmer,[1,†] Jacob Teeter,[1] Wonhee Ko,[1] Cui-Zu Chang,[3] Panchapakesan Ganesh,[1,‡] and An-Ping Li[1,§]

[1]*Center for Nanophase Materials Sciences, Oak Ridge National Laboratory, Oak Ridge, Tennessee 37831, USA*

[2]*Department of Materials Science and Engineering, University of Tennessee, Knoxville, Tennessee 37916, USA*

[3]*Department of Physics, The Pennsylvania State University, University Park, Pennsylvania 16802, USA*

[4]*Department of Physics, North Carolina State University, Raleigh, North Carolina 27695, USA*

[5]*Computational Sciences and Engineering Division, Oak Ridge National Laboratory, Oak Ridge, Tennessee 37916, USA*

(Received 22 January 2021; revised 2 November 2021; accepted 6 December 2021; published 20 January 2022)

The interplay of nontrivial band topology and magnetism gives rise to a series of exotic quantum phenomena, such as the emergent quantum anomalous Hall (QAH) effect and topological magnetoelectric effect. Many of these quantum phenomena have local manifestations when the global symmetry is broken. Here, we report local signatures of the thickness-dependent topology in intrinsic magnetic topological insulator $MnBi_2Te_4$ (MBT), using scanning tunneling microscopy and spectroscopy on molecular beam epitaxy grown MBT thin films. A thickness-dependent band gap is revealed, which we reproduce with theoretical calculations. Our theoretical results indicate a topological quantum phase transition beyond a film thickness of one monolayer, with alternating QAH and axion insulating states for odd and even layers, respectively. At step edges, we observe localized electronic states, in general agreement with axion insulator and QAH edge states, respectively, indicating topological phase transitions across the steps. The demonstration of thickness-dependent topological properties highlights the role of nanoscale control over novel quantum states, reinforcing the necessity of thin film technology in quantum information science applications.

DOI: 10.1103/PhysRevB.105.035423

Topological insulators (TIs), such as Bi_2Te_3, have an inverted band gap which leads to topologically protected Dirac-like surface states [1–4]. By introducing magnetism into a topological insulator, the time-reversal-symmetry of the system is broken and a magnetic exchange gap opens at its Dirac point [5]. When the chemical potential is tuned into this magnetic exchange gap, the quantum anomalous Hall (QAH) effect with dissipationless chiral edge transport appears. The QAH effect has been experimentally realized in magnetically doped $Bi_{2-x}Sb_xTe_3$ thin films [6,7]. However, it has become clear that the random distribution of dopants (e.g., Cr or V) can lead to inhomogeneous magnetic exchange gaps [8] and, more importantly for thin films, local chemical potential fluctuations [9], which undermine the promises of the unique electronic properties for potential applications.

Recently, it was shown that stoichiometric $MnBi_2Te_4$ (MBT) provides an alternative way to realize a magnetic TI. In contrast to a TI with randomly distributed magnetic dopants, MBT has an ordered crystal structure in which the magnetic moments are arranged in layers with an A-type antiferromagnetic (AFM) ordering [10–14]. As a result, MBT promises a bigger magnetic exchange gap and more uniform chemical potential than magnetically doped TIs [13,15,16]. More interestingly, MBT thin films exhibit alternating topological phases as their thickness decreases. In MBT thin films with an odd number of layers, a zero magnetic field QAH state has been theoretically predicted [11,17] and experimentally demonstrated in transport measurements [16,18,19]. In contrast, the axion insulator state, which is characterized by a vanishing Chern number but has a finite topological Chern-Simons term, was claimed to be realized in thin films with an even number of layers [20]. However, while the local electronic structure of bulk MBT crystals has been studied in detail with scanning probe techniques [21–24], the thickness-dependent variations of electronic properties of the MBT thin films remain elusive. Especially, how a symmetry breaking introduced by thickness changes will affect the quantum states in MBT remains to be explored.

Here, we report the structural and spectroscopic characterization of epitaxial MBT thin films by scanning tunneling microscopy/spectroscopy (STM/S) in combination with first-principles theoretical modeling to examine the thickness-dependent electronic properties, which underpin the reported QAH and axion insulator states. Moreover, we report the observation of edge states as a local manifestation of symmetry breaking, which also allows us to infer the magnetic structure of the MBT film. MBT films with a nominal thickness t of several septuple layers (SL) are grown on a bilayer graphene

*Present address: Peter Grünberg Institut (PGI-3), Forschungszentrum Jülich, 52425 Jülich, Germany.

†Present address: Ames Laboratory - U.S. Department of Energy, Ames, Iowa 50011, USA.

‡ganeshp@ornl.gov

§apli@ornl.gov

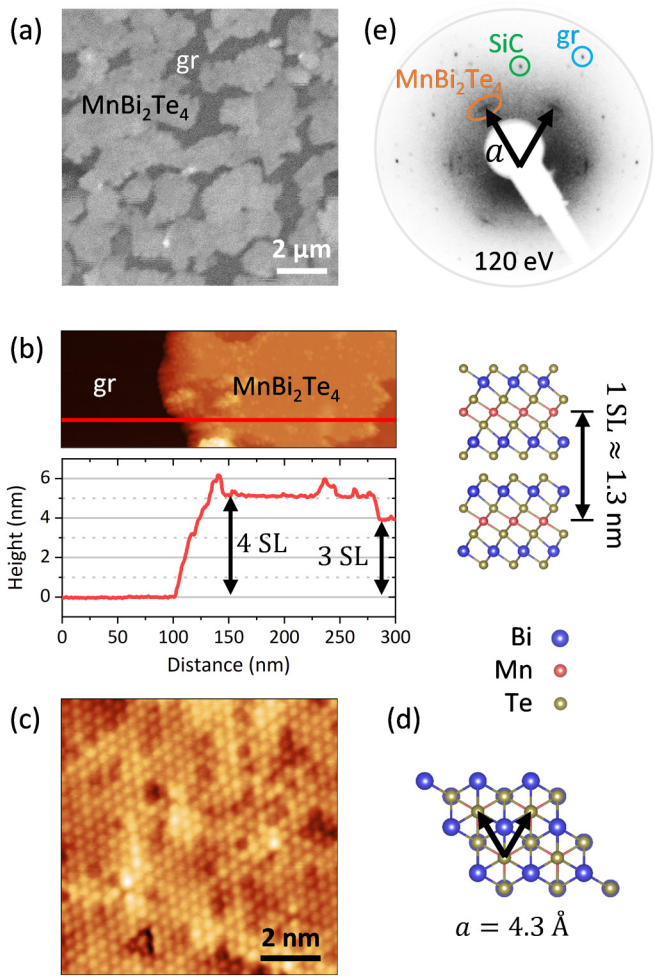

FIG. 1. Epitaxial $MnBi_2Te_4$ thin films on bilayer graphene terminated SiC. (a) Scanning electron micrograph of the sample showing an island growth mode on the graphene (gr)/SiC substrate. (b) Scanning tunneling micrograph of a $MnBi_2Te_4$ island with different thicknesses (top), height profile along the indicated line (bottom) and atomic model of $MnBi_2Te_4$ with indicated layer-to-layer distance. (c) Atomic resolution tunneling image acquired on an island showing a hexagonal lattice with lattice constant $a = 4.3$ Å. (d) Top view of the $MnBi_2Te_4$ lattice with indicated lattice vectors corresponding to the spacing of the topmost Te layer. (e) Low-energy electron diffraction pattern showing streaks corresponding to $a = 4.3$ Å, indicating a variation in the island orientation around a preferred alignment with the graphene lattice.

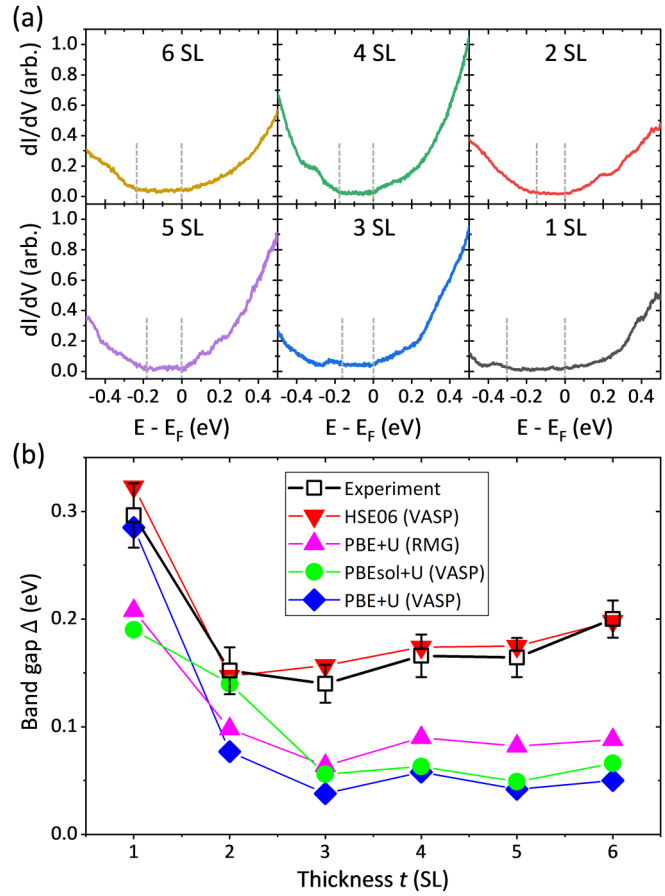

FIG. 2. Thickness-dependent electronic structure of $MnBi_2Te_4$. (a) Tunneling conductance measured on $MnBi_2Te_4$ islands of different thickness with valence and conduction band edges determined from fitting log-scale spectra (see the Supplemental Material). (b) Thickness-dependent experimental band gaps and comparison to theoretical calculations using different kinds of functionals (HSE06 values reported with exact exchange fractions reported in Table I). Independent of the functional used for the calculations, the band gap is topological (inverted) above $\geqslant 2$ SL thickness.

terminated 6H-SiC(0001) substrate by molecular beam epitaxy. The growth procedure consists of alternating deposition of Bi_2Te_3 and MnTe layers followed by annealing as reported in Ref. [15]. After the growth, samples are capped with ~10 nm of Te and transferred to a combined scanning electron microscope (SEM)/STM chamber (Omicron LT Nanoprobe) where the Te capping layer is removed by annealing the sample at ~250 °C in UHV for 60 min. The subsequent STM/S measurements are performed at 4.6 K.

SEM measurements of the decapped sample show island growth [Fig. 1(a)]. Large area STM scans [Fig. 1(b)] reveal MBT island thicknesses in multiples of $t = (13 \pm 0.3)$ Å = 1 SL. Atomic resolution scans on the islands show a hexagonal lattice with lattice constant $a = 4.3$ Å [Fig. 1(c)], consistent with the Te plane at the MBT surface [Fig. 1(d)] and in agreement with measurements on MBT bulk crystals [24]. Furthermore, low-energy electron diffraction (LEED) measurements on the thin film [Fig. 1(e)] show circularly elongated spots corresponding to $a = 4.3$ Å, in addition to the well-known graphene/SiC substrate spots [25]. The MBT spots indicate a preferred rotational alignment of the MBT with the graphene substrate. From the width of the MBT spots, we determine the alignment of the MBT islands with respect to the substrate to have a standard deviation of ~6.4° (see Supplemental Material [26]).

Systematic scanning tunneling spectroscopy studies of the MBT islands with thicknesses ranging from 1 SL to 6 SL [Fig. 2(a)] show overall similarity to spectra taken on bulk MBT crystals [24] but are shifted in energy and varying in the gap sizes. Due to large step heights, partly mobile islands and mobile adsorbates on the surface, STS experiments were difficult, limiting the amount of available spectra at each layer

TABLE I. Band gaps Δ, exact exchange values α and moments per Mn atom as function of layer thickness t determined by fit of HSE06 hybrid functional calculations to the experimental data.

t (SL)	1	2	3	4	5	6
Δ (meV)	323	147	157	174	175	198
α (%)	10	10	35	37	25	43
μ_B/Mn	4.27	4.26	4.47	4.48	4.41	4.51

thickness. Independent of the layer thickness, we find that the conduction band edges of the films are located near the Fermi energy E_F. This band shift can be attributed to the same lattice defects that render bulk MBT electron doped, particularly Te vacancies and antisite defects [23,51]. This observation is also in agreement with other vdW thin films grown on graphene/SiC substrates [40]. Our results further show a systematic change of the MBT island band gap sizes as function of their layer thickness. The extracted band gaps [Fig. 2(b)] show a sharp decrease in gap size from 1 SL (∼296 meV) to 2 SL (∼152 meV), followed by a gradual increase of the band gap up to ∼200 meV for 6 SL (the thickest film studied here). Interestingly, odd layers tend to show slightly smaller gaps while even layers show slightly bigger gaps within the error bars. Indeed, for $S \geqslant 2$ SL we find that a linear fit results in a sum of squared residuals of 572 meV, while the residual with respect to our HSE calculations is only 332 meV, i.e., the latter is statistically more likely to be correct. The sizes of the observed gaps generally agree well with recent photoemission experiments [52], but are significantly larger than theoretically predicted gaps [17]. Possible explanations for a nonzero dI/dV signal inside some of the gaps include tip-induced band bending, in-gap defect states and a not entirely gapped surface state, similar to observations on MBT bulk crystals [24].

To capture the experimental trend and obtain a quantitative comparison of the measured band gaps, we performed density functional theory (DFT) calculations with improved treatment of nonlocal exchange and correlation effects, which allow us to explore the sensitivity of thin film band gaps to interlayer separation, as well as local magnetic moments. A summary of our calculations is shown in Fig. 2(b) alongside the experimental data. Using Perdew-Burke-Ernzerhof (PBE) functionals and a Hubbard U of 4 eV, our theoretical calculations qualitatively reproduce the trend of our experiments (for details on the calculations see the Supplemental Material). Interestingly, even when using the same DFT-D3 type dispersion correction and Hubbard U [41,42], we find that the interlayer distances obtained from PBE are generally larger than those obtained from the PBEsol functional by ∼0.5 Å, with the PBE interlayer separation tending towards the bulk value of 13.6 Å [43] for 6 SL (Fig. S2). However, for thicknesses of 3 to 4 SL, the PBEsol+U functional [44], which is an improved functional for solids, predicts the interlayer distance to be close to 13.1 Å, which is in better agreement with our experimentally measured layer thickness of (13.0 ± 0.3) Å. Consequently, due to different vdW interlayer distances, there are quantitative differences in the band gaps as function of thickness. Overall, we find that for thicknesses of 3 SL and

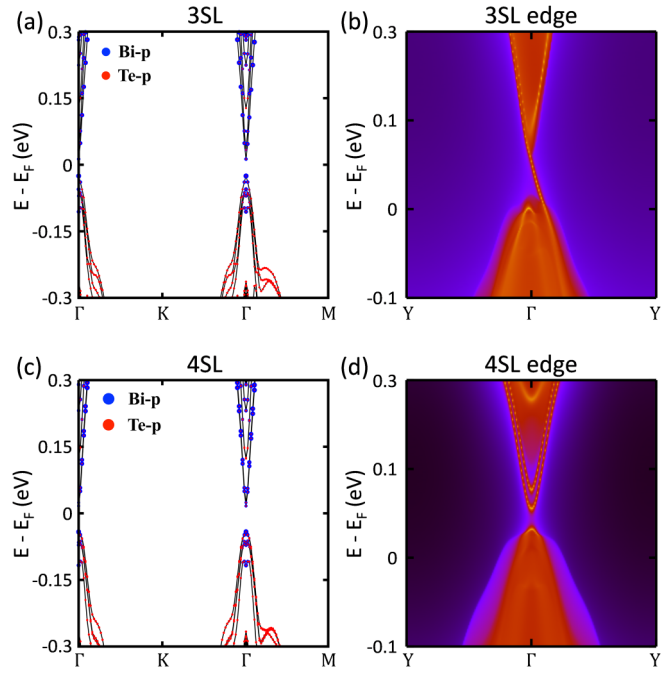

FIG. 3. Calculated band structure and edge states of a 3 SL and 4 SL $MnBi_2Te_4$ film. (a) Bulk band structure of 3 SL film with (b) a gapless QAH edge state which crosses the band gap. (c) Bulk band structure of 4 SL film with (d) a topologically trivial edge state with a gap. Symbol sizes in (a) and (c) indicate strength of the orbital contribution to the eigenvalue spectrum.

4 SL, the structures with smaller interlayer separation, obtained from PBEsol+U, show a larger gap than the ones obtained from PBE+U. Using a real-space code (RMG-DFT [45–47]) with harder pseudopotentials, we find a similar trend for the band gaps as from our plane-wave VASP calculations. For both, PBE+U and PBEsol+U, even layers show a larger gap than odd layers, due to the antiferromagnetic ordering, which results in uncompensated moments in odd layers. This even-odd oscillatory behavior on the bandgap is consistent with our experiments and is reduced with increasing layer thickness as expected in the thermodynamic limit. We note that for $t \geqslant 1$ SL the spin-orbit coupling and exchange gaps dominate the opening of the band gap. Quantitatively though, PBE/PBEsol+U functionals still significantly underestimate the gaps observed in the experiments.

To resolve this discrepancy, we resort to the more computationally expensive Heyd-Scuseria-Ernzerhof-type hybrid functionals (HSE06) [48–50], which includes a varying degree of exact exchange interaction to the total potential, to capture nonlocal effects in the correlation of electrons with the same spin. From calculations with the hybrid functional approach, we find that adding the exact exchange generally results in larger gaps than obtained from PBE+U and PBEsol+U (see the Supplemental Material for details). As a result, by varying the exact exchange, we can fit the band gaps obtained from PBEsol+U+D3 to the experimental gap data, resulting in the values listed in Table I. These results directly indicate that the thinner films (1 SL and 2 SL) have ∼0.2 μ_B lower local moment per Mn atom compared to the thicker films (3 to 6 SL), which are close to the theoretical bulk value

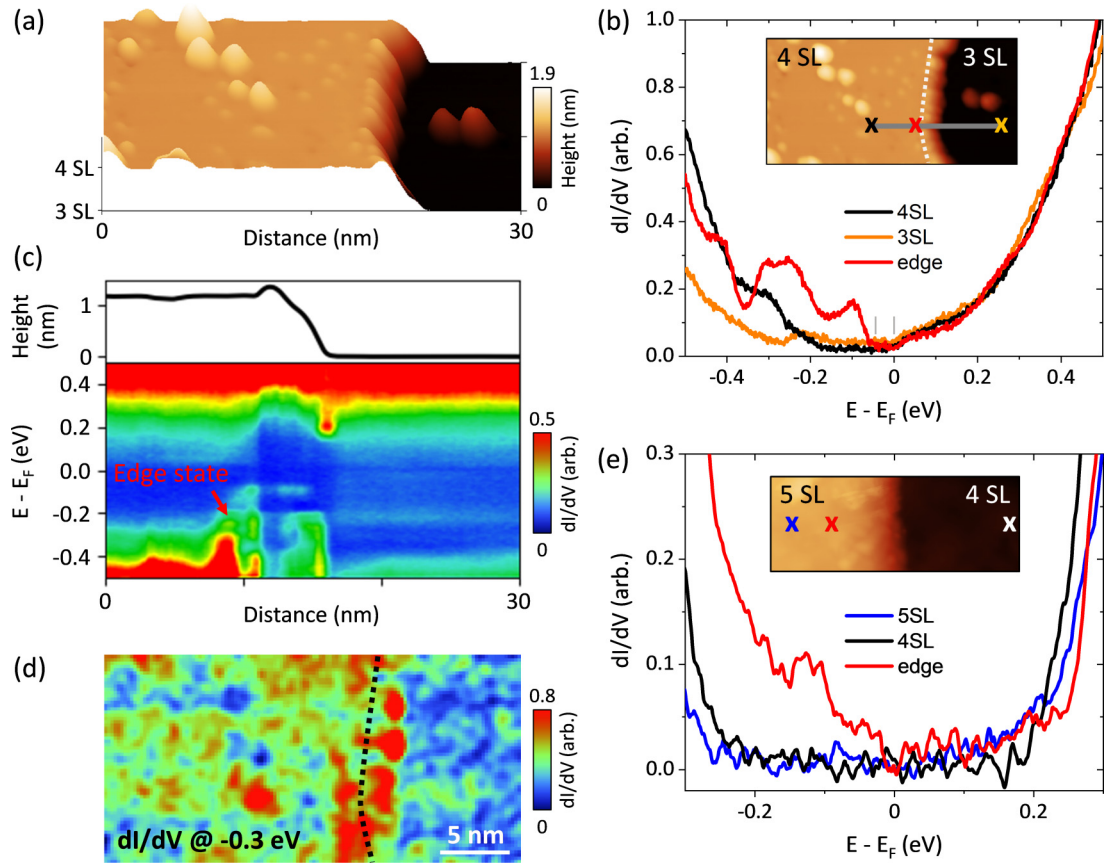

FIG. 4. Observation of edge states. (a) Topography of a 4 SL-3 SL step edge. (b) Tunneling conductance at different locations across the step as indicated in the inset. Away from the edge, the spectra on the terraces correspond to the spectra shown in Fig. 2. Near the position of the edge (indicated as dashed line in the inset) an additional density of states is observed, indicating the presence of an edge state. Stabilization parameters: $E - E_F = 0.5$ V, $I_t = 100$ pA. (c) Tunneling spectra taken along the line indicated in the inset in (b) aligned with the height profile along the same line. The increased density of states of the edge state feature is visible on top of the flat terrace in vicinity to the topographic edge. (d) Intensity map of the tunneling conductance at $E - E_F = -0.3$ eV showing the spectral feature of the edge state along the edge. (e) Same as (b) but for a 5 SL-4 SL step edge.

(∼4.51 μ_B per Mn), as detailed in the Supplemental Material. Our calculated moments are in the range of reported bulk magnetic moments [12,13] (see the Supplemental Material for more details). Even layers in general have similar sized or higher moments per Mn atom, than the thinner odd layers, thus explaining the larger gaps observed on the even layers compared to the odd layer due to the overall antiferromagnetic ordering.

Independent of the employed functionals, our calculations show a sharp decrease of the band gap from 1 to 2 SL followed by the opening of an inverted gap for $\geqslant$2 SL. This inverted band gap gives rise to QAH and axion insulator phases in odd and even layers, respectively. We calculated the resulting edge states in a 3 and 4 SL film (Fig. 3). For a 3 SL film, the uncompensated magnetic moments result in the breaking of time reversal symmetry, which gives rise to a topologically protected gapless edge state, namely, the QAH edge state. In contrast, for a 4-SL film, the combination of preserved time-reversal-symmetry and half translation symmetry ($T\Theta_{1/2}$) results in an edge state that is not topologically protected and for which our DFT calculations predict a gap of 20 meV. We explore the latter edge state experimentally by studying a 4 SL-3 SL step edge [Fig. 4(a)]. STS measurements across the step edge [Fig. 4(b)] show the presence of an increased dI/dV signal on the 4 SL terrace, next to the topographic position of the step edge. The spectroscopic signature of this edge state is an increased density of states in the energy range -0.35 eV $\leqslant$ E $\leqslant$ 0 eV, i.e., extending into the $\Delta \approx 175$ meV band gap observed on the 4 SL terrace. The lateral extension of the edge state into the 4 SL terrace is ∼1.5 nm [Fig. 4(c)]. In qualitative agreement with our calculations, this edge state has a gap of $\Delta \approx 55$ meV, which is located at the Fermi energy. In differential conductance maps corresponding to the edge state energy $E - E_F = -300$ meV, we find that the edge state extends along the topographic step of the 4 SL terrace [Fig. 4(d)], similar to the case of, e.g., the quantum spin Hall edge state in WTe_2 [40,53]. The observation of the gapped edge state in the 4 SL film indicates an AFM alignment between the layers such that the individual layer's magnetic moments are compensated, because if the film had a net magnetic moment we would expect a gapless QAH edge state based on theory. In combination with the remarkable agreement between our film thickness-dependent theoretical calculations of the electronic structure with our experimental STS data, we therefore conclude that the observed edge state feature is the manifestation of the axion

insulator edge state. In comparison, the edge state observed at a 5 SL-4 SL step edge is expected to show metallic behavior, yet we still observe a small gap of ∼10 mV near E_F [Fig. 4(e)]. This small gap at E_F could be indicative of a Tomonaga-Luttinger liquid behavior in the metallic edge state, which results in an algebraic suppression of the tunneling density of states towards E_F, similar to those observed in QSH edge states in other systems [40,53,54]. To determine the underlying nature of the observed gap warrants further study. We note that the measurement of the 5-SL edge state suffers from a somewhat insulating tip, but was reproducible. Additional data can be found in the Supplemental Material.

In conclusion, we have demonstrated the local manifestation of QAH and axion insulator phases in MBT thin films with varying thickness. The observation of a gapped edge state at an even-odd layer step edge and nearly metallic edge state at odd-even steps supports the existence of the axion and QSH phase. A temperature-dependent study of the local electronic structure of MBT thin films could provide further insight into the nature of the surface and edge states, as a transition to a 3D TI is expected above the Néel temperature. In combination with *s*-wave superconductivity, the QAH and axion state in MBT thin films provide a route towards the realization of Majorana zero modes for topological quantum computing [55]. Lastly, we note that we observe an overall larger fraction of even layer thicknesses than odd layers in our samples. This observation indicates that MBT films with even layer thicknesses are energetically favored during the film growth, likely due to their compensated magnetic moments. This finding could possibly be exploited to achieve uniform film thicknesses for applications.

From a theoretical point of view, the improved agreement of our calculations with experiments, by variation of the exact exchange for different thicknesses, suggests a complicated interplay between electronic correlations, magnetism, and hybridization. This makes MBT an interesting benchmark system to validate a variety of theoretical methods beyond the conventional DFT approach such as the dynamic mean field theory and quantum Monte Carlo methods [56]. Furthermore, while plane-wave DFT-methods do not allow explicit simulations of step-edges, we demonstrate that DFT methods using multiresolution real-space grids are suitable for large-scale simulations [45–47], which agree well with plane-wave codes and enable calculations of edge states for arbitrary film thicknesses in future studies.

This research was conducted at the Center for Nanophase Materials Sciences, which is a Department of Energy (DOE) Office of Science User Facility. F.L. acknowledges funding from the Alexander von Humboldt foundation through a Feodor Lynen postdoctoral fellowship. A.D.P.'s initial calculations were financially supported by the Oak Ridge National Laboratory's Laboratory Directed Research and Development project (Project ID No.7448, PI: P.G.). Subsequent computations by A.D.P. were supported by the U.S. DOE, Office of Science, Basic Energy Sciences, Materials Sciences and Engineering Division, as part of the Computational Materials Sciences Program and Center for Predictive Simulation of Functional Materials. The VASP calculations used resources of the National Energy Research Scientific Computing Center (NERSC), a U.S. DOE Office of Science User Facility operated under Contract No. DE-AC02-05CH11231. All computations using WANNIER90 code used resources of the Computer and Data Environment for Science (CADES) at the Oak Ridge National Laboratory, which is supported by the Office of Science of the U.S. DOE under Contract No. DE-AC05-00OR22725. The development of RMG was funded by the DOE Exascale Computing Project and the National Science Foundation Grant No. OAC-1740309. RMG based computations used resources of the Oak Ridge Leadership Computing Facility at the Oak Ridge National Laboratory, which is supported by the Office of Science of the U.S. DOE under Contract No. DE-AC05-00OR22725. The film growth done at Penn State is supported by the Gordon and Betty Moore Foundation's EPiQS Initiative (Grant No. GBMF9063 to C.Z.C.) and ARO Young Investigator Program Award (W911NF1810198). A portion of the research (A.-P.L.) is supported by the U.S. DOE, Office of Science, National Quantum Information Science Research Centers.

[1] Y. L. Chen, J. G. Analytis, J.-H. Chu, Z. K. Liu, S.-K. Mo, X. L. Qi, H. J. Zhang, D. H. Lu, X. Dai, Z. Fang, S. C. Zhang, I. R. Fisher, Z. Hussain, and Z.-X. Shen, Science **325**, 178 (2009).

[2] H. Zhang, C.-X. Liu, X.-L. Qi, X. Dai, Z. Fang, and S.-C. Zhang, Nat. Phys. **5**, 438 (2009).

[3] M. Z. Hasan and C. L. Kane, Rev. Mod. Phys. **82**, 3045 (2010).

[4] X.-L. Qi and S.-C. Zhang, Rev. Mod. Phys. **83**, 1057 (2011).

[5] Y. L. Chen, J. H. Chu, J. G. Analytis, Z. K. Liu, K. Igarashi, H. H. Kuo, X. L. Qi, S. K. Mo, R. G. Moore, D. H. Lu, M. Hashimoto, T. Sasagawa, S. C. Zhang, I. R. Fisher, Z. Hussain, and Z. X. Shen, Science **329**, 659 (2010).

[6] C.-Z. Chang, J. Zhang, X. Feng, J. Shen, Z. Zhang, M. Guo, K. Li, Y. Ou, P. Wei, L.-L. Wang, Z.-Q. Ji, Y. Feng, S. Ji, X. Chen, J. Jia, X. Dai, Z. Fang, S.-C. Zhang, K. He, Y. Wang, L. Lu, X.-C. Ma, and Q.-K. Xue, Science **340**, 167 (2013).

[7] C. Z. Chang, W. Zhao, D. Y. Kim, H. Zhang, B. A. Assaf, D. Heiman, S. C. Zhang, C. Liu, M. H. W. Chan, and J. S. Moodera, Nat. Mater. **14**, 473 (2015).

[8] I. Lee, C. K. Kim, J. Lee, S. J. L. Billinge, R. Zhong, J. A. Schneeloch, T. Liu, T. Valla, J. M. Tranquada, G. Gu, and J. C. S. Davis, Proc. Natl. Acad. Sci. **112**, 1316 (2015).

[9] J. Dai, D. West, X. Wang, Y. Wang, D. Kwok, S. W. Cheong, S. B. Zhang, and W. Wu, Phys. Rev. Lett. **117**, 106401 (2016).

[10] D. Zhang, M. Shi, T. Zhu, D. Xing, H. Zhang, and J. Wang, Phys. Rev. Lett. **122**, 206401 (2019).

[11] J. Li, Y. Li, S. Du, Z. Wang, B. L. Gu, S. C. Zhang, K. He, W. Duan, and Y. Xu, Sci. Adv. **5**, eaaw5685 (2019).

[12] M. M. Otrokov, I. I. Klimovskikh, H. Bentmann, D. Estyunin, A. Zeugner, Z. S. Aliev, S. Gaß, A. U. B. Wolter, A. V. Koroleva, A. M. Shikin, M. Blanco-Rey, M. Hoffmann, I. P. Rusinov, A. Y. Vyazovskaya, S. V. Eremeev, Y. M. Koroteev, V.

M. Kuznetsov, F. Freyse, J. Sánchez-Barriga, I. R. Amiraslanov, M. B. Babanly, N. T. Mamedov, N. A. Abdullayev, V. N. Zverev, A. Alfonsov, V. Kataev, B. Büchner, E. F. Schwier, S. Kumar, A. Kimura, L. Petaccia, G. Di Santo, R. C. Vidal, S. Schatz, K. Kißner, M. Ünzelmann, C. H. Min, S. Moser, T. R. F. Peixoto, F. Reinert, A. Ernst, P. M. Echenique, A. Isaeva, and E. V. Chulkov, Nature (London) **576**, 416 (2019).

[13] J. Q. Yan, Q. Zhang, T. Heitmann, Z. Huang, K. Y. Chen, J. G. Cheng, W. Wu, D. Vaknin, B. C. Sales, and R. J. McQueeney, Phys. Rev. Materials **3**, 064202 (2019).

[14] P. Rani, A. Saxena, R. Sultana, V. Nagpal, S. S. Islam, S. Patnaik, and V. P. S. Awana, J. Supercond. Novel Magn. **32**, 3705 (2019).

[15] Y. Gong, J. Guo, J. Li, K. Zhu, M. Liao, X. Liu, Q. Zhang, L. Gu, L. Tang, X. Feng, D. Zhang, W. Li, C. Song, L. Wang, P. Yu, X. Chen, Y. Wang, H. Yao, W. Duan, Y. Xu, S.-C. Zhang, X. Ma, Q.-K. Xue, and K. He, Chin. Phys. Lett. **36**, 076801 (2019).

[16] Y. Deng, Y. Yu, M. Z. Shi, Z. Guo, Z. Xu, J. Wang, X. H. Chen, and Y. Zhang, Science **367**, 895 (2020).

[17] M. M. Otrokov, I. P. Rusinov, M. Blanco-Rey, M. Hoffmann, A. Y. Vyazovskaya, S. V. Eremeev, A. Ernst, P. M. Echenique, A. Arnau, and E. V. Chulkov, Phys. Rev. Lett. **122**, 107202 (2019).

[18] D. Ovchinnikov, X. Huang, Z. Lin, Z. Fei, J. Cai, T. Song, M. He, Q. Jiang, C. Wang, H. Li, Y. Wang, Y. Wu, D. Xiao, J.-H. Chu, J. Yan, C.-Z. Chang, Y.-T. Cui, and X. Xu, Nano Lett. **21**, 2544 (2021).

[19] Y.-F. Zhao, L.-J. Zhou, F. Wang, G. Wang, T. Song, D. Ovchinnikov, H. Yi, R. Mei, K. Wang, M. H. W. Chan, C.-X. Liu, X. Xu, and C.-Z. Chang, Nano Lett. **21**, 7691 (2021).

[20] C. Liu, Y. Wang, H. Li, Y. Wu, Y. Li, J. Li, K. He, Y. Xu, J. Zhang, and Y. Wang, Nat. Mater. **19**, 522 (2020).

[21] Y. Yuan, X. Wang, H. Li, J. Li, Y. Ji, Z. Hao, Y. Wu, K. He, Y. Wang, Y. Xu, W. Duan, W. Li, and Q.-K. Xue, Nano Lett. **20**, 3271 (2020).

[22] Z. Liang, A. Luo, M. Shi, Q. Zhang, S. Nie, J. J. Ying, J. F. He, T. Wu, Z. Wang, G. Xu, Z. Wang, and X. H. Chen, Phys. Rev. B **102**, 161115(R) (2020).

[23] Z. Huang, M.-H. Du, J. Yan, and W. Wu, Phys. Rev. Materials **4**, 121202(R) (2020).

[24] W. Ko, M. Kolmer, J. Yan, A. D. Pham, M. Fu, F. Lüpke, S. Okamoto, Z. Gai, P. Ganesh, and A.-P. Li, Phys. Rev. B **102**, 115402 (2020).

[25] N. Briggs, B. Bersch, Y. Wang, J. Jiang, R. J. Koch, N. Nayir, K. Wang, M. Kolmer, W. Ko, A. De La Fuente Duran, S. Subramanian, C. Dong, J. Shallenberger, M. Fu, Q. Zou, Y.-W. Chuang, Z. Gai, A.-P. Li, A. Bostwick, C. Jozwiak, C.-Z. Chang, E. Rotenberg, J. Zhu, A. C. T. van Duin, V. Crespi, and J. A. Robinson, Nat. Mater. **19**, 637 (2020).

[26] See Supplemental Material at http://link.aps.org/supplemental/10.1103/PhysRevB.105.035423 for additional STM, LEED, and DFT data sets, as well as further details on the theoretical calculations, which includes Refs. [12,13,27–50].

[27] S. H. Lee, Y. Zhu, Y. Wang, L. Miao, T. Pillsbury, H. Yi, S. Kempinger, J. Hu, C. A. Heikes, P. Quarterman, W. Ratcliff, J. A. Borchers, H. Zhang, X. Ke, D. Graf, N. Alem, C.-Z. Chang, N. Samarth, and Z. Mao, Phys. Rev. Research **1**, 012011(R) (2019).

[28] H. Fu, C.-X. Liu, and B. Yan, Sci. Adv. **6**, eaaz0948 (2020).

[29] S. Grimme, J. Antony, S. Ehrlich, and H. Krieg, J. Chem. Phys. **132**, 154104 (2010).

[30] S. Grimme, S. Ehrlich, and L. Goerigk, J. Comput. Chem. **32**, 1456 (2011).

[31] A. A. Mostofi, J. R. Yates, Y.-S. Lee, I. Souza, D. Vanderbilt, and N. Marzari, Comput. Phys. Commun. **178**, 685 (2008).

[32] Q. Wu, S. Zhang, H.-F. Song, M. Troyer, and A. A. Soluyanov, Comput. Phys. Commun. **224**, 405 (2018).

[33] P. Poulopoulos, S. Baskoutas, S. D. Pappas, C. S. Garoufalis, S. A. Droulias, A. Zamani, and V. Kapaklis, J. Phys. Chem. C **115**, 14839 (2011).

[34] J. Q. Yan, S. Okamoto, M. A. McGuire, A. F. May, R. J. McQueeney, and B. C. Sales, Phys. Rev. B **100**, 104409 (2019).

[35] Y.-J. Hao, P. Liu, Y. Feng, X.-M. Ma, E. F. Schwier, M. Arita, S. Kumar, C. Hu, R. e. Lu, M. Zeng, Y. Wang, Z. Hao, H.-Y. Sun, K. Zhang, J. Mei, N. Ni, L. Wu, K. Shimada, C. Chen, Q. Liu, and C. Liu, Phys. Rev. X **9**, 041038 (2019).

[36] L. Ding, C. Hu, F. Ye, E. Feng, N. Ni, and H. Cao, Phys. Rev. B **101**, 020412(R) (2020).

[37] A. Dal Corso and A. Mosca Conte, Phys. Rev. B **71**, 115106 (2005).

[38] K. Laasonen, R. Car, C. Lee, and D. Vanderbilt, Phys. Rev. B **43**, 6796 (1991).

[39] D. R. Hamann, Phys. Rev. B **88**, 085117 (2013).

[40] S. Tang, C. Zhang, D. Wong, Z. Pedramrazi, H.-Z. Tsai, C. Jia, B. Moritz, M. Claassen, H. Ryu, S. Kahn, J. Jiang, H. Yan, M. Hashimoto, D. Lu, R. G. Moore, C.-C. Hwang, C. Hwang, Z. Hussain, Y. Chen, M. M. Ugeda, Z. Liu, X. Xie, T. P. Devereaux, M. F. Crommie, S.-K. Mo, and Z.-X. Shen, Nat. Phys. **13**, 683 (2017).

[41] S. L. Dudarev, G. A. Botton, S. Y. Savrasov, C. J. Humphreys, and A. P. Sutton, Phys. Rev. B **57**, 1505 (1998).

[42] J. P. Perdew, K. Burke, and M. Ernzerhof, Phys. Rev. Lett. **77**, 3865 (1996).

[43] H. Li, S. Liu, C. Liu, J. Zhang, Y. Xu, R. Yu, Y. Wu, Y. Zhang, and S. Fan, PCCP **22**, 556 (2020).

[44] J. P. Perdew, A. Ruzsinszky, G. I. Csonka, O. A. Vydrov, G. E. Scuseria, L. A. Constantin, X. Zhou, and K. Burke, Phys. Rev. Lett. **100**, 136406 (2008).

[45] E. L. Briggs, D. J. Sullivan, and J. Bernholc, Phys. Rev. B **54**, 14362 (1996).

[46] http://www.rmgdft.org/.

[47] M. Hodak, S. Wang, W. Lu, and J. Bernholc, Phys. Rev. B **76**, 085108 (2007).

[48] A. V. Krukau, O. A. Vydrov, A. F. Izmaylov, and G. E. Scuseria, J. Chem. Phys. **125**, 224106 (2006).

[49] J. Heyd and G. E. Scuseria, J. Chem. Phys. **121**, 1187 (2004).

[50] J. Heyd, G. E. Scuseria, and M. Ernzerhof, J. Chem. Phys. **118**, 8207 (2003).

[51] M.-H. Du, J. Yan, V. R. Cooper, and M. Eisenbach, Adv. Funct. Mater. **31**, 2006516 (2021).

[52] C. X. Trang, Q. Li, Y. Yin, J. Hwang, G. Akhgar, I. Di Bernardo, A. Grubišić-Čabo, A. Tadich, M. S. Fuhrer, S.-K. Mo, N. Medhekar, and M. T. Edmonds, ACS Nano **15**, 13444 (2020).

[53] F. Lüpke, D. Waters, S. C. de la Barrera, M. Widom, D. G. Mandrus, J. Yan, R. M. Feenstra, and B. M. Hunt, Nat. Phys. **16**, 526 (2020).

[54] R. Stühler, F. Reis, T. Müller, T. Helbig, T. Schwemmer, R. Thomale, J. Schäfer, and R. Claessen, Nat. Phys. **16**, 47 (2020).

[55] M. Kayyalha, D. Xiao, R. Zhang, J. Shin, J. Jiang, F. Wang, Y.-F. Zhao, R. Xiao, L. Zhang, K. M. Fijalkowski, P. Mandal, M. Winnerlein, C. Gould, Q. Li, L. W. Molenkamp, M. H. W. Chan, N. Samarth, and C.-Z. Chang, Science **367**, 64 (2020).

[56] P. Ganesh, F. Lechermann, I. Kylänpää, J. T. Krogel, P. R. C. Kent, and O. Heinonen, Phys. Rev. B **101**, 155129 (2020).